Quantum Monte Carlo study of quantized muon in molecular systems

Li Deng [1,2] Yue Yuan,[3] Ziwen Pan [3] Liangwen Chen,[1,2,4,*] and Lei Yang[1,2,4]

[1]*Advanced Energy Science and Technology Guangdong Laboratory, Huizhou 516000, China*

[2]*Institute of Modern Physics, CAS, Lanzhou 730000, China*

[3]*State Key Laboratory of Particle Detection and Electronics, University of Science and Technology of China, Hefei 230026, China*

[4]*School of Nuclear Science and Technology, University of Chinese Academy of Sciences, Beijing 100049, China*

(Received 22 May 2024; revised 8 July 2024; accepted 30 August 2024; published 10 September 2024)

In muon spin relaxation/rotation/resonance (μSR) technology, positive muons serve as local spin probes for detecting electron-muon or nucleus-muon spin interactions. Given that a muon's mass is approximately one-ninth that of a proton, its zero-point energy significantly influences μSR experiments. The straightforward application of the Born-Oppenheimer approximation fails to adequately address the muon's behavior from an *ab initio* perspective. Despite previous efforts to correct for the quantum effects of the muon, existing approximations often fall short, yielding unsatisfactory results. This paper addresses these limitations by focusing on the many-body system of quantized muons in materials and directly solving the muon-included many-body equation using quantum Monte Carlo techniques. We further simulate the hyperfine couplings of the muon, demonstrating that this rigorous approach can produce accurate results and explicit error margins. This method proves beneficial for μSR experiment analysis and holds potential for broader application in studying the quantum effects of heavy, positively charged particles in various materials.

DOI: 10.1103/PhysRevB.110.115118

I. INTRODUCTION

The study of multibody systems involving positively charged particles and electrons presents a significant and versatile challenge across various scientific disciplines, including positron annihilation spectroscopy, muon spin relaxation/rotation/resonance (μSR), and hydrogen nuclei behavior in materials. Given the identical mass of electrons and positrons, the wave function of positrons is treated on equal footing with electrons. Two-component density functional theory (TCDFT) [1–4], along with the use of quantum Monte Carlo (QMC) for simulating essential two-body functionals [5,6], stands as the predominant method. However, as the particle mass increases, such as with muons or protons, the interaction distance between these particles and electrons reduces, rendering the local spin approximation (LDA) and its improvements such as the generalized gradient approximation (GGA) ineffective. Furthermore, the Born-Oppenheimer approximation (pointlike muon [7,8]) and its corrections, such as vibrational methods [9–11] and double adiabatic approximations [12–15], often rely on limited or unverified assumptions and currently are difficult to provide theoretical predictions that align accurately with experimental data. Given the significant quantum effects due to the muon's mass—merely one-ninth that of a proton—an accurate and robust method becomes crucial not only for μSR analysis but also for understanding the behavior of heavy positively charged particles in materials.

An essential method for addressing the quantum effects of the muon involves directly solving the muon-included many-body Schrödinger equation. QMC is ideally suited for this task as it can solve the many-body equation without relying on empirical parameters, and the quality of the calculated results can be clearly reflected by the QMC simulation itself. Recent advancements have enabled the successful integration of the positron as a quantized particle within QMC frameworks [16], paving the way for similar calculations with quantized muons, despite differences between the orbitals of localized muons and diffusion positrons. In this paper, we treat muons as quantized particles and incorporate their wave functions into the overall many-body wave function. We employ both variational Monte Carlo (VMC) [17] and diffusion Monte Carlo (DMC) [18] to perform numerical solutions, ensuring the natural inclusion of muon quantum effects. We also estimated the observable muon hyperfine couplings and found that QMC predictions closely align with experimental data. Given its accurate results and explicit error range, this method is not only promising for further investigations into muons but is also applicable to other heavy positively charged particles.

II. METHOD

What we are considering is a many-body Schrödinger equation of a muon in material,

$$\hat{H}[\psi(r_1,\ldots,r_N;r_\mu)] = E\psi(r_1,\ldots,r_N;r_\mu), \tag{1}$$

where r_i are the coordinates of the ith electron, r_μ are the coordinates of the muon, and

$$\hat{H} = \sum_i -\frac{1}{2}\nabla_{e,i}^2 - \frac{1}{2m_\mu}\nabla_\mu^2 + \frac{1}{2}\sum_{i\neq j}\frac{1}{|r_i - r_j|} - \sum_i \frac{1}{|r_i - r_\mu|} - \sum_{i,j} V_{\text{ion}}^-(r_i, R_j) + \sum_j V_{\text{ion}}^+(r_\mu, R_j), \tag{2}$$

*Contact author: chenlw@impcas.ac.cn

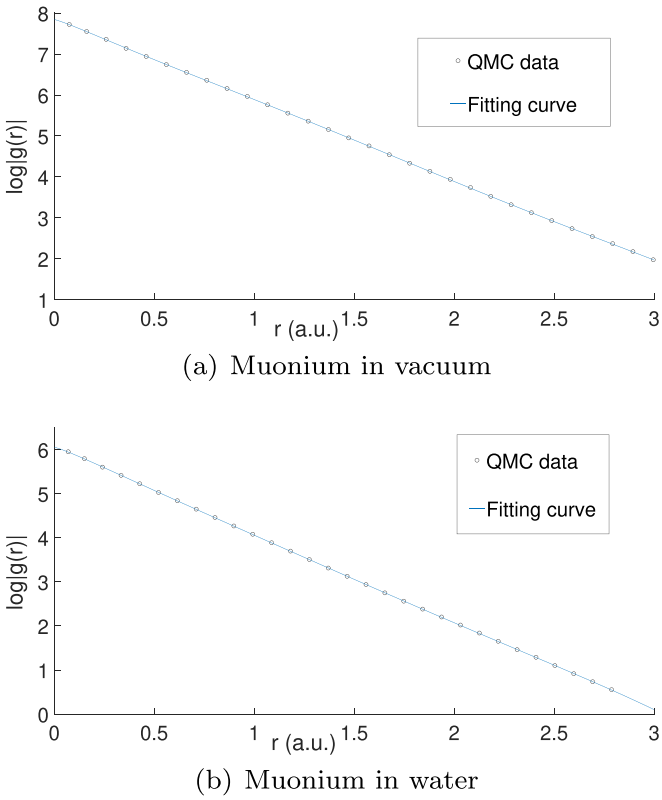

FIG. 1. Representative $g_\uparrow(r)$ results for muonium in (a) vacuum and (b) water.

where m_μ is the mass of the muon, R_j are the coordinates of the jth ion, V_{ion}^- and V_{ion}^+ are the potential from the ions to electrons and the muon, respectively, and both are defined as a positive value.

To solve Eq. (1) by QMC, it is essential to employ parametrized trial wave functions for both electrons and muons (one-particle orbitals). In general, the trial wave function of electrons can be generated by the density functional theory (DFT) with a pointlike muon model (DFT+μ [19]), which provides a reliable starting point for highly localized muons. However, the orbital configuration of the muon has not been extensively studied previously. Our approach involves setting a Gaussian distribution for the muon density in real space (using either a Gaussian sigma or the maximum muon density value as the variable) and employing a fast Fourier transform to convert this distribution into a plane-wave form. This plane wave is then transformed into the blip form [20] for practical computations. We observed that if the initial maximum muon density is set within a reasonable range (0.5–10 a.u.), the VMC optimization calculations tend to converge satisfactorily (give stable enough total energy and variance results although the VMC optimization steps and the final Jastrow exponents are different), otherwise the VMC optimization may fall into a wrong local result with high total energy and variance.

TABLE I. VMC energy results of muonium in vacuum when changing the simulation cell volume. $r_s = (3/4\pi n)^{1/3}$, and $n = 2/V$ is the average density. r_s is in unit of a.u. while E_{VMC} is in unit of a.u. per particle. The $g(0)$ results are gotten from the system of $r_s = 10.0$.

r_s	1.0	2.0	4.0
	6.0	8.0	10.0
	12.0	15.0	20.0
	30.0	40.0	50.0
E_{VMC}	−0.72601(4)	−0.38719(1)	−0.26019(6)
	−0.25077(3)	−0.2495646(5)	−0.24917944(3)
	−0.24901675(3)	−0.2489091(1)	−0.24884410(1)
	−0.248810771(1)	−0.2488026629(2)	−0.24879977558(2)

TABLE II. VMC energy (in a.u.) and $g(r)$ results of muonium in benzene. Nstep is the vmc_equil_nstep of the VMC calculation while vmc_nstep is set to be 1/5 of the vmc_equil_nstep.

Nstep	Total energy	Var.	The first five $g_\uparrow(r)$
1×10^4	−37.88(3)	1.38(9)	96.5;63.6;32.8;31.3;24.1
1×10^5	−37.87(1)	1.42(3)	83.5;59.7;70.3;49.5;48.2
1×10^6_1[a]	−37.860(3)	1.41(1)	87.7;81.9;63.2;55.4;47.2
1×10^6_2[a]	−37.851(3)	1.398(8)	97.9;74.8;63.6;54.4;46.6
1×10^7_1[a]	−37.8507(9)	1.485(13)	93.0;76.5;64.8;54.5;46.6
1×10^7_2[a]	−37.8508(9)	1.548(19)	87.3;75.5;64.7;54.8;46.5
1×10^7_3[a]	−37.8503(8)	1.448(9)	89.5;79.2;65.6;55.0;46.8

[a]The expanded number 1, 2 and 3 of Nstep represent the identifier of the calculation with the same VMC configuration.

After having the trial orbitals of the muon and electron, the composition form of the many-body wave function should be determined. Under the Slater-Jastrow-backflow (SJB) scheme [21,22], the many-body wave function of the system can be expressed as

$$\Psi^{\text{SJB}} = e^{J(\mathbf{R})}\phi_\mu(\mathbf{r}_\mu + \xi(\mathbf{R})) \times [\phi_i(\mathbf{r}_\uparrow + \xi(\mathbf{R}))] \cdot [\phi_j(\mathbf{r}_\downarrow + \xi(\mathbf{R}))], \quad (3)$$

where $\mathbf{R}$ are the positions of all the particles, ϕ are the one-particle orbitals, i and j stand for up and down electrons, respectively, $[\cdots]$ denotes a Slater determinant, $J(\mathbf{R})$ are the Jastrow exponents, and $\xi(\mathbf{R})$ is the backflow displacement. The Jastrow exponents are written as [23]

$$J(\mathbf{R}) = \sum_{i=1}^{N-1}\sum_{j=i+1}^{N} u(r_{ij}) + \sum_{I=1}^{N_{\text{ions}}}\sum_{i=1}^{N} \chi_I(r_{iI}) + \sum_{I=1}^{N_{\text{ions}}}\sum_{i=1}^{N-1}\sum_{j=i+1}^{N} f_I(r_{iI}, r_{jI}, r_{ij}) + \sum_{i=1}^{N-1}\sum_{j=i+1}^{N} p(\mathbf{r}_{ij}), \quad (4)$$

where N is the total number of all quantized particles (electrons and the muon), and N_{ions} is the total number of ions in materials. The Jastrow exponents in Eq. (4) are the sum of the u term (isotropic functions of electron-electron separation), χ term (isotropic functions of electron-ion separations), f term (isotropic functions of electron-electron and electron-ion separations), and p term (plane-wave expansions in electron-electron separations). In this work, we find that the VMC optimization with backflow displacement $\xi(\mathbf{R})$ is unstable and does not improve the wave function (there may be technical problems in the backflow optimization of the quantized muon

TABLE III. QMC results. Energy and the variances of VMC are in a.u. per simulation cell (except for the vacuum case, where the energy is in a.u. per particle). The values and error bars of $g(0)$ and hyperfine couplings are determined by the ten data sets while the energy and variance are displayed by just one of the ten data sets.

Material	E_{VMC}	Var. of VMC	E_{DMC}	$g_{\uparrow}(0)$	$g_{\downarrow}(0)$	A_{QMC}	$A_{\mathrm{DFT}+\mu}$[a]	A_{expt}
Vacuum	−0.24917944(10)	$4(4)\times10^{-10}$	−0.24917952(3)	2550(100)		4350(170) MHz	4711 MHz	4463 MHz
Water	−17.51(3)	1.89(11)	−17.700(4)	423(6)	0	4480(60) MHz	4656 MHz	4432(1) MHz [32][b]
Acetone	−36.75(4)	2.99(12)	−37.1141(24)	112(4)	123(3)	−50(70) MHz	−27.2 MHz	6.8(2) MHz [37]
Benzene	−37.87(3)	1.39(8)	−38.112(3)	100.7(22)	91.9(20)	490(60) MHz	500.7 MHz	526(1) MHz [38]
TTF	−76.32(4)	3.29(19)	−77.612(4)	178(5)	168(4)	280(50) MHz	268.6 MHz	≃300 MHz [39]

[a]Projector augmented-wave (PAW) and its reconstruction method [36] calculated by QE.
[b]Measured at room temperature, only for reference.

system), so the Slater-Jastrow (SJ) wave function ($\xi = 0$) is simply applied. Further study on the effect of the backflow will be conducted in the future work.

Considering the observable measurement, the hyperfine couplings A can be expressed as

$$A = \frac{2\mu_0}{3}\gamma_e\gamma_\mu\rho_s(\mathbf{r}_\mu), \tag{5}$$

where γ_e and γ_μ are the gyromagnetic ratio of the electron and the muon, respectively, μ_0 is the magnetic permeability of vacuum, and $\rho_s(\mathbf{r}_\mu)$ is the spin density (up density minus down density) of electrons at the muon site. In the case of the quantized muon, $\rho_s(\mathbf{r}_\mu)$ can be written as

$$\begin{aligned}\rho_s(\mathbf{r}_\mu) &= \left[\sum_i^{N_\uparrow}\frac{\langle\Psi|\hat{O}_i^{\uparrow}\delta(\mathbf{r}_i-\mathbf{r}_\mu)|\Psi\rangle}{\langle\Psi\mid\Psi\rangle}\right.\\ &\quad\left.-\sum_i^{N_\downarrow}\frac{\langle\Psi|\hat{O}_i^{\downarrow}\delta(\mathbf{r}_i-\mathbf{r}_\mu)|\Psi\rangle}{\langle\Psi\mid\Psi\rangle}\right]\\ &= [N_\uparrow g_\uparrow(0) - N_\downarrow g_\downarrow(0)]/V,\end{aligned} \tag{6}$$

where g is the rotationally and translationally averaged pair-correlation function (PCF), V is the volume of the simulation cell, and $\hat{O}_i$ is the spin-projection operator. After the Jastrow exponents are optimized using the VMC variance-minimum scheme [24], the DMC calculation is employed and the PCFs are simulated from the DMC calculation directly (see below for not doing a 2DMC-VMC extrapolation). The $g(r)$ is simply obtained by binning the interparticle distance sample of the PCF, thus the rotationally and translationally averaged PCF at zero distance, $g(0)$, can be estimated by an extrapolation of $g(r)$. In order to obtain small fitting errors in a simpler form, all $g(r)$ values are modeled using the following polynomial fit,

$$\begin{aligned}\log|g(r)| &= a_0 - r + a_{15}\cdot r^{1.5} + a_2\cdot r^2 + a_3\cdot r^3\\ &\quad + a_4\cdot r^4 + a_5\cdot r^5.\end{aligned} \tag{7}$$

The fitting range is chosen to be 0–2.5 a.u. because we are only interested in $g(0)$ and the $g(r)$ within this range is smooth enough. After the $g(0)$ is extrapolated and the statistical errors are estimated by the standard deviation of data sets (see below), then the final hyperfine couplings are calculated through Eqs. (5) and (6).

III. RESULTS AND DISCUSSION

A. Muonium in vacuum

In contrast to muon-in-material systems, muonium in vacuum behaves as a homogeneous fluid, making the methodologies discussed previously inapplicable. Instead, a constant plane-wave wave function is utilized directly as the single-particle orbital in SJB calculations [25]. Although it is very different from the actual materials, we still calculated it as the most special case. The CASINO package [26] is applied in all QMC calculations of this paper. The calculation of muonium in vacuum is employed by periodic cubic cells with various total density. First, the finite-size error is checked (as shown in Table I), and the results demonstrate that as the system size increases, the total energy reliably converges to the precise isolated muonium energy. The corresponding $g(0)$ value can be extrapolated from the $g(r)$ data, as detailed in Fig. 1 [just one of the ten data sets, see below (details for obtaining $g(r)$ and $g(0)$ are in Sec. II)]. The $g(r)$ results in vacuum are obtained from the calculation of $r_s = 10$ a.u. since the $g(r)$ becomes stable when $r_s > 8$ a.u.

In order to obtain reasonable error bars, we employed each calculation ten times, by using the same set of Jastrow parameters and repeating the VMC and DMC calculations. The final error bars of $g(0)$ and hyperfine couplings were determined by the standard deviation of these ten data sets. The time step of DMC was set at 0.01 a.u. with a target weight 1000.0. Note that a smaller DMC time step may influence the total energy of the system (about 0.01 a.u.), but the influence on $g(0)$ is found to be smaller than its statistical error. A more rigorous calculation may require the extrapolation to $dt = 0$. Consequently, the resulting $g(0)$ was 2550(100) and the hyperfine couplings were estimated to be 4.35(17) GHz, as detailed in Table III. For comparison, experimental data recorded 4463 MHz and pointlike muon DFT calculations provided 4711 MHz. It is important to note that while more precise results might be obtainable through a 2DMC-VMC extrapolation [27], in this work the statistical error of $g_{\mathrm{VMC}}(0)$ is at least two times larger than that of $g_{\mathrm{DMC}}(0)$ because the $g(r)$ results of the VMC calculation fluctuate obviously even if the steps of VMC are large enough (see Table II), thus performing a 2DMC-VMC extrapolation would increase the final error bars of hyperfine couplings by ∼3 times. Consequently, this study relies directly on the results from DMC calculations.

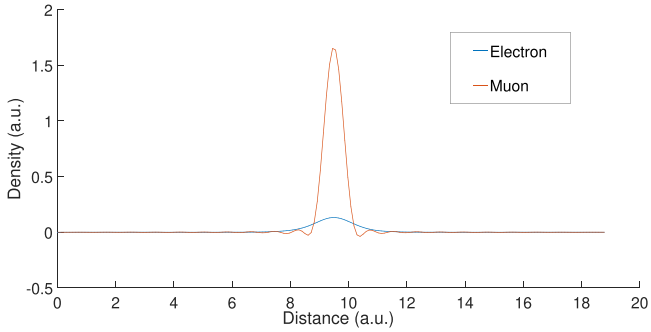

(a)

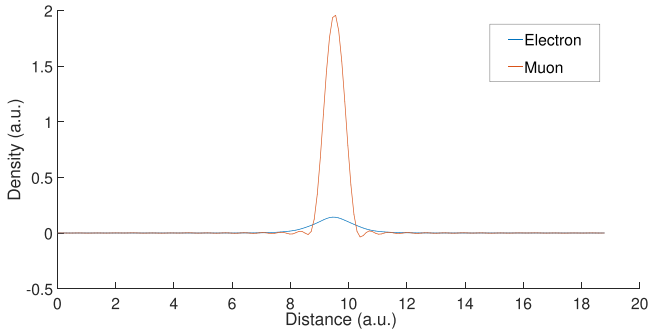

(b)

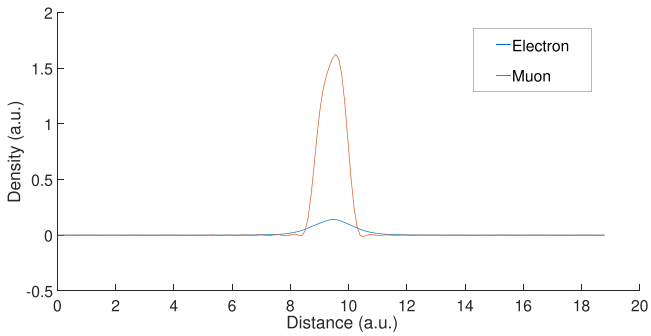

(c)

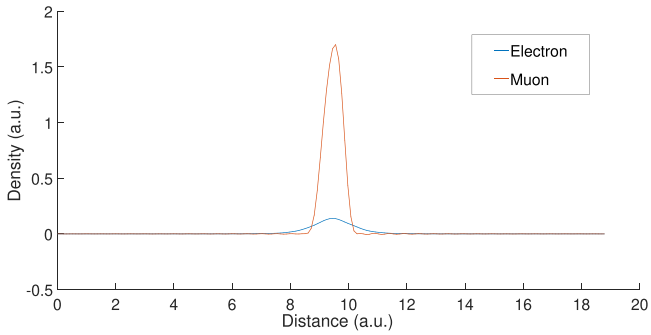

(d)

FIG. 2. The density of the muon and the electrons in water, for cutoff (a) 30.0 a.u., (b) 50.0 a.u., (c) 62.5 a.u., and (d) 80.0 a.u. Plotted along the x axis centered on the average muon site.

B. Interstitial muonium in water

The DFT calculations indicate that in liquid water, muons do not participate in bonding but exist freely from water molecules as interstitial muoniums [28]. However, the presence of water molecules still confines muons in localized states, rather than allowing them to diffuse, which is crucial for analyzing the muon distribution density at low local potentials. In this study, we employed norm-conserving, nonlocal Dirac-Fock average relativistic effective

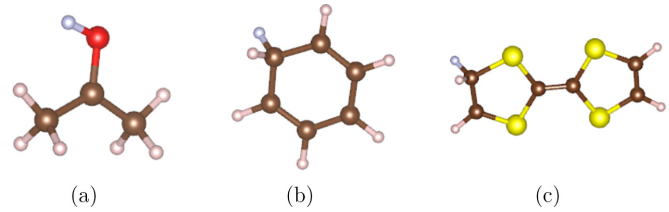

(a) (b) (c)

FIG. 3. Structures of muon in (a) acetone C_3H_6OMu, (b) benzene C_6H_6Mu, and (c) TTF $C_6S_4H_4Mu$. Muons are shown as gray circles.

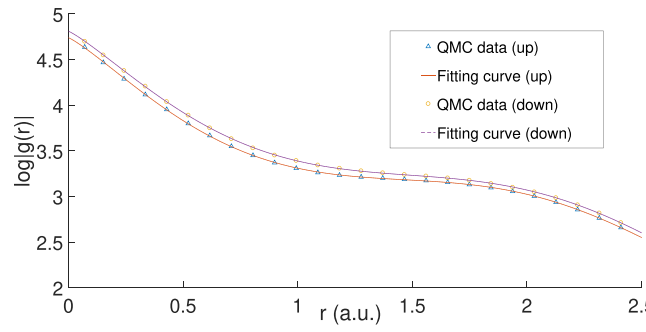

(a)

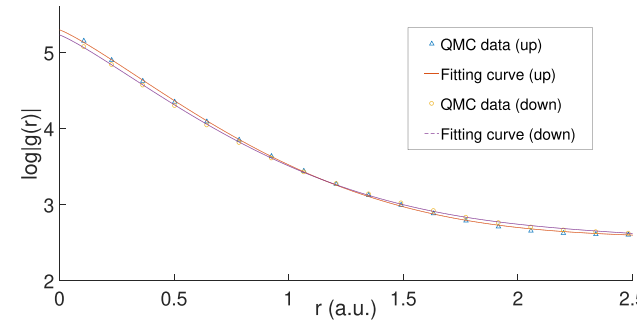

(b)

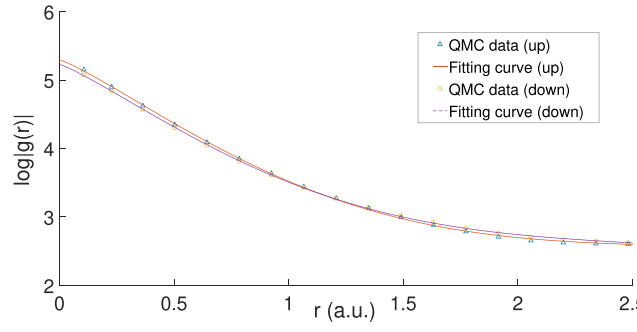

(c)

FIG. 4. Representative $g(r)$ results for (a) acetone, (b) benzene, and (c) TTF. Fitted as Eq. (7).

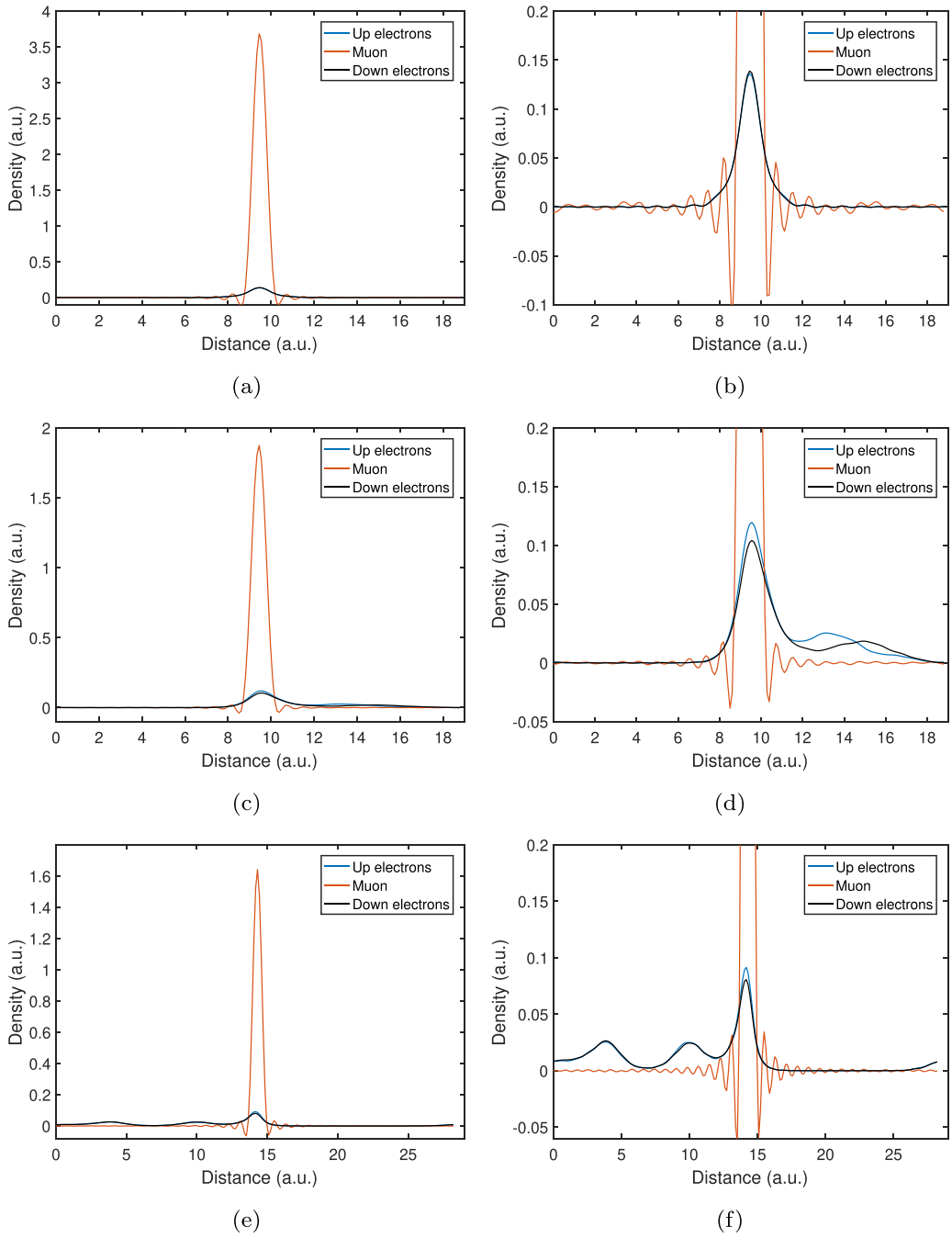

FIG. 5. Densities for (a), (b) acetone, (c), (d) benzene, and (e), (f) TTF. Cutoffs are set to be 30.0 a.u. Plotted along the x axis centered on the average muon site.

pseudopotentials (AREPs) [29,30] for the atoms within the material. The DFT calculations were conducted using the QUANTUM ESPRESSO (QE) package [31] and, with electron orbitals generated in plane-wave form via the pw2casino.x subroutine. Subsequently, the muon orbital, after being converted to a plane wave, was added to the orbital file, which was then transformed into blip style for use in the CASINO simulations. Additionally, we introduced a nucleus with $Z = 0$ (ghost atom) at the average muon site to facilitate the use of the χ term and f term of the Jastrow factor as outlined in Eq. (4). This would be helpful for improving the quality of the wave function.

The calculation was done within a periodic cubic cell of 10 Å lattice constant, where the muon is placed far enough from the water molecules. First, we simulated the $g(0)$, obtaining a value of 423(6), with one representative $g(r)$ result depicted in Fig. 1. The final hyperfine couplings were 4.48(6) GHz, closely aligning with the experimental data recorded at 4432(1) MHz [32]. Note that the experiment is done at room temperature, the thermal effects are not included in the calculation, and the comparison is just a rough reference. Additionally, we attempted to characterize the density distribution of the muon, a challenging task as the output density in CASINO, expanded by the plane wave, fluctuates significantly

with low cutoffs and incurs higher computational costs at high cutoffs.

For interstitial muonium in water, we explored muon density under various cutoff thresholds, as illustrated in Fig. 2. The muon density calculations, performed independently of $g(0)$, do not influence the hyperfine couplings. Despite the potential inaccuracy in absolute density values, the calculated local density of the muon substantially exceeds that predicted by the double adiabatic approximation [14,15] and vibrational method [9,33], yet remains below the results obtained from TCDFT with the LDA two-body functional for a muon-electron homogeneous system [25]. These discrepancies merit further discussion and analysis.

C. Bonding muons in organic molecules

A more common situation of a muon in material is the bonding muons, which occurs not only in organic molecules but also in crystal lattices. In order to simplify the calculation, in this paper we performed calculations for the following three organic molecules: acetone, benzene, and TTF. Their muon-containing structures are shown in Fig. 3, which are calculated by DFT+μ structure optimization, using the QE package with the Perdew-Burke-Ernzerhof (PBE) functional [34] and optimized norm conserving Vanderbilt (ONCV) [35] pseudopotentials (such a condition is only used for structure optimization calculation, not for the one-particle orbital generation, as discussed in the previous section).

To assess the finite-size effect, we adjusted the lattice constants for benzene, acetone, and TTF and observed that QMC results stabilize [the changes of the energy and the $g(0)$ when increasing the cell size would not be larger than the reported statistical uncertainty] when the lattice constant reaches at least 10 Å for benzene and acetone, and 15 Å for TTF (cubic cell). The lattice size mentioned above, 10 or 15 Å, is actually used in our calculation. The results for $g(0)$ and hyperfine couplings are detailed in Table III, with corresponding $g(r)$ values and muon densities illustrated in Figs. 4 and 5, respectively.

The output density cutoff was set at 30 a.u. to facilitate the conceptual explanation of muon density without affecting the electron density or the hyperfine coupling results. The hyperfine coupling outcomes align with experimental values within the established error margins. Compared to DFT+μ and its correction methods, in QMC the quality of the trial wave function and the error margins of observable measurements can be clearly revealed. While the relative error for $g(0)$ remains under 5%, the relative error for hyperfine couplings may be significantly larger due to the averaging offset. This discrepancy does not arise with positrons since their annihilation rate correlates directly with the total electron density, rather than the spin density. The limitations in improving the statistical accuracy of $g(0)$—primarily due to the considerable errors inherent in VMC and DMC calculations—preclude further extrapolations using 2DMC-VMC. Consequently, employing QMC for low hyperfine coupling materials might be restricted, marking a notable limitation of this methodology currently.

IV. CONCLUSION

In this paper, we directly solved the muon-included many-body Schrödinger equation for molecular systems using QMC and simulated the hyperfine couplings of the muon. This approach allows for an essential consideration of the muon's quantum effects and enables clear identification of the errors in both the trial wave function and the observable measurements. The calculated hyperfine couplings are well aligned with experimental results within the stated error bars, although the calculated muon density distribution deviates from existing approximations. The primary limitation of QMC in this context is the statistical error associated with $g(0)$, particularly impacting the accuracy of low hyperfine coupling calculations. Improvements in QMC calculations could be achieved by refining the trial wave function, especially the muon orbital. Given its precise handling of quantum effects, this method holds significant potential for studying muons and other heavy positively charged particles.

ACKNOWLEDGMENTS

This work was financially supported by the National Natural Science Foundation of China (Grant No. 12105327), the National Natural Science Foundation of China (Grant No. 12005221), and the Guangdong Basic and Applied Basic Research Foundation (Grant No. 2023B1515120067). Computing resources were mainly provided by the supercomputing system in the Dongjiang Yuan Intelligent Computing Center. The authors would like to thank N. D. Drummond from the Department of Physics, Lancaster University for valuable discussion.

[1] M. J. Puska and R. M. Nieminen, Theory of positrons in solids and on solid surfaces, Rev. Mod. Phys. **66**, 841 (1994).

[2] R. M. Nieminen, E. Boronski, and L. J. Lantto, Two-component density-functional theory: Application to positron states, Phys. Rev. B **32**, 1377(R) (1985).

[3] E. Boroński and R. M. Nieminen, Electron-positron density-functional theory, Phys. Rev. B **34**, 3820 (1986).

[4] J. Wiktor, G. Jomard, and M. Torrent, Two-component density functional theory within the projector augmented-wave approach: Accurate and self-consistent computations of positron lifetimes and momentum distributions, Phys. Rev. B **92**, 125113 (2015).

[5] N. D. Drummond, P. L. Ríos, R. J. Needs, and C. J. Pickard, Quantum Monte Carlo study of a positron in an electron gas, Phys. Rev. Lett. **107**, 207402 (2011).

[6] B. Barbiellini and J. Kuriplach, Proposed parameter-free model for interpreting the measured positron annihilation spectra of materials using a generalized gradient approximation, Phys. Rev. Lett. **114**, 147401 (2015).

[7] J. Möller, P. Bonfà, D. Ceresoli, F. Bernardini, S. Blundell, T. Lancaster, R. De Renzi, N. Marzari, I. Watanabe, S. Sulaiman *et al.*, Playing quantum hide-and-seek with the muon: Localizing muon stopping sites, Phys. Scr. **88**, 068510 (2013).

[8] I. J. Onuorah, P. Bonfà, and R. De Renzi, Muon contact hyperfine field in metals: A DFT calculation, Phys. Rev. B **97**, 174414 (2018).

[9] J. S. Möller, D. Ceresoli, T. Lancaster, N. Marzari, and S. J. Blundell, Quantum states of muons in fluorides, Phys. Rev. B **87**, 121108(R) (2013).

[10] I. J. Onuorah, P. Bonfà, R. De Renzi, L. Monacelli, F. Mauri, M. Calandra, and I. Errea, Quantum effects in muon spin spectroscopy within the stochastic self-consistent harmonic approximation, Phys. Rev. Mater. **3**, 073804 (2019).

[11] R. H. Luchsinger, Y. Zhou, and P. F. Meier, Gradient corrections in first-principles calculations of hyperfine parameters in semiconductors, Phys. Rev. B **55**, 6927 (1997).

[12] K. R. Brorsen, Y. Yang, and S. Hammes-Schiffer, Multicomponent density functional theory: Impact of nuclear quantum effects on proton affinities and geometries, J. Phys. Chem. Lett. **8**, 3488 (2017).

[13] Y. Yang, K. R. Brorsen, T. Culpitt, M. V. Pak, and S. Hammes-Schiffer, Development of a practical multicomponent density functional for electron-proton correlation to produce accurate proton densities, J. Chem. Phys. **147**, 114113 (2017).

[14] M. Goli and S. Shahbazian, Two-component density functional theory for muonic molecules: Inclusion of the electron–positive muon correlation functional, J. Chem. Phys. **156**, 044104 (2022).

[15] N. S. Riyahi, M. Goli, and S. Shahbazian, Quantifying errors of electron-proton/muon correlation functionals through the Kohn-Sham inversion of a two-component model system, Phys. Rev. B **108**, 245155 (2023).

[16] K. A. Simula, J. E. Muff, I. Makkonen, and N. D. Drummond, Quantum Monte Carlo study of positron lifetimes in solids, Phys. Rev. Lett. **129**, 166403 (2022).

[17] D. M. Ceperley and B. J. Alder, Ground state of the electron gas by a stochastic method, Phys. Rev. Lett. **45**, 566 (1980).

[18] W. Foulkes, L. Mitas, R. Needs, and G. Rajagopal, Quantum Monte Carlo simulations of solids, Rev. Mod. Phys. **73**, 33 (2001).

[19] S. J. Blundell and T. Lancaster, DFT+μ: Density functional theory for muon site determination, Appl. Phys. Rev. **10**, 021316 (2023).

[20] D. Alfè and M. J. Gillan, Efficient localized basis set for quantum Monte Carlo calculations on condensed matter, Phys. Rev. B **70**, 161101(R) (2004).

[21] Y. Kwon, D. M. Ceperley, and R. M. Martin, Effects of backflow correlation in the three-dimensional electron gas: Quantum Monte Carlo study, Phys. Rev. B **58**, 6800 (1998).

[22] P. López Ríos, A. Ma, N. D. Drummond, M. D. Towler, and R. J. Needs, Inhomogeneous backflow transformations in quantum Monte Carlo calculations, Phys. Rev. E **74**, 066701 (2006).

[23] N. D. Drummond, M. D. Towler, and R. J. Needs, Jastrow correlation factor for atoms, molecules, and solids, Phys. Rev. B **70**, 235119 (2004).

[24] C. J. Umrigar, J. Toulouse, C. Filippi, S. Sorella, and R. G. Hennig, Alleviation of the fermion-sign problem by optimization of many-body wave functions, Phys. Rev. Lett. **98**, 110201 (2007).

[25] L. Deng, Y. Yuan, F. L. Pratt, W. Zhang, Z. Pan, and B. Ye, Two-component density functional theory study of quantized muons in solids, Phys. Rev. B **107**, 094433 (2023).

[26] R. J. Needs, M. D. Towler, N. D. Drummond, P. López Ríos, and J. R. Trail, Variational and diffusion quantum Monte Carlo calculations with the CASINO code, J. Chem. Phys. **152**, 154106 (2020).

[27] I. Gurtubay, R. Gaudoin, and J. M. Pitarke, Benchmark quantum Monte Carlo calculations of the ground-state kinetic, interaction and total energy of the three-dimensional electron gas, J. Phys.: Condens. Matter **22**, 065501 (2010).

[28] T. E. Markland, S. Habershon, and D. E. Manolopoulos, Quantum diffusion of hydrogen and muonium atoms in liquid water and hexagonal ice, J. Chem. Phys. **128**, 194506 (2008).

[29] J. Trail and R. Needs, Smooth relativistic Hartree-Fock pseudopotentials for H to Ba and Lu to Hg, J. Chem. Phys. **122**, 174109 (2005).

[30] J. Trail and R. Needs, Norm-conserving Hartree-Fock pseudopotentials and their asymptotic behavior, J. Chem. Phys. **122**, 014112 (2005).

[31] P. Giannozzi, S. Baroni, N. Bonini, M. Calandra, R. Car, C. Cavazzoni, D. Ceresoli, G. L. Chiarotti, M. Cococcioni, I. Dabo *et al.*, QUANTUM ESPRESSO: A modular and open-source software project for quantum simulations of materials, J. Phys.: Condens. Matter **21**, 395502 (2009).

[32] I. McKenzie, H. Dilger, E. Roduner, R. Scheuermann, and U. Zimmermann, Solvation of a hydrogen isotope in aqueous methanol, NaCl, and KCl solutions, J. Phys. Chem. B **112**, 3070 (2008).

[33] M. Gomilšek, F. L. Pratt, S. P. Cottrell, S. J. Clark, and T. Lancaster, Many-body quantum muon effects and quadrupolar coupling in solids, Commun. Phys. **6**, 142 (2023).

[34] J. P. Perdew, K. Burke, and M. Ernzerhof, Generalized gradient approximation made simple, Phys. Rev. Lett. **77**, 3865 (1996).

[35] D. R. Hamann, Optimized norm-conserving Vanderbilt pseudopotentials, Phys. Rev. B **88**, 085117 (2013).

[36] P. E. Blöchl, Projector augmented-wave method, Phys. Rev. B **50**, 17953 (1994).

[37] F. L. Pratt (unpublished).

[38] D. G. Fleming, D. J. Arseneau, M. Y. Shelley, B. Beck, H. Dilger, and E. Roduner, μSR studies of hyperfine couplings and molecular interactions of the Mu-cyclohexadienyl radical in Y-zeolites and in solid bulk benzene, J. Phys. Chem. C **115**, 11177 (2011).

[39] F. Pratt, S. Blundell, T. Jestädt, B. W. Lovett, R. Macrae, and W. Hayes, Muon radical states in some electron donor and acceptor molecules, Magn. Reson. Chem. **38**, S27 (2000).